115 PW–850 J compressed beam demonstration using the PETAL facility

N. Blanchot, G. Behar, J.C. Chapuis, C. Chappuis, S. Chardavoine, J.F. Charrier, H. Coïc, C. Damiens-Dupont, J. Duthu, Garcia P., et al.

Research Article | Vol. 25, No. 15 | 24 Jul 2017 | OPTICS EXPRESS 16957
Optics EXPRESS

1.15 PW–850 J compressed beam demonstration using the PETAL facility

N. BLANCHOT,* G. BÉHAR, J.C. CHAPUIS, C. CHAPPUIS, S. CHARDAVOINE, J.F. CHARRIER, H. COÏC, C. DAMIENS-DUPONT, J. DUTHU, P. GARCIA, J. P. GOOSSENS, F. GRANET, C. GROSSET-GRANGE, P. GUERIN, B. HEBRARD, L. HILSZ, L. LAMAIGNERE, T. LACOMBE, E. LAVASTRE, T. LONGHI, J. LUCE, F. MACIAS, M. MANGEANT, E. MAZATAUD, B. MINOU, T. MORGAINT,S. NOAILLES, J. NEAUPORT, P. PATELLI, E. PERROT-MINNOT, C. PRESENT, B. REMY, C. ROUYER, N. SANTACREU, M. SOZET, D. VALLA, AND F. LANIESSE

Commissariat à l'énergie atomique et aux énergies alternatives – Centre d'études scientifiques et techniques d'aquitaine, F- 33116 LE BARP, France
**nathalie.blanchot@cea.fr*

Abstract: The Petawatt Aquitaine Laser (PETAL) facility was designed and constructed by the French Commissariat à l'énergie atomique et aux énergies alternatives (CEA) as an additional PW beamline to the Laser MegaJoule (LMJ) facility. PETAL energy is limited to 1 kJ at the beginning due to the damage threshold of the final optics. In this paper, we present the commissioning of the PW PETAL beamline. The first kJ shots in the amplifier section with a large spectrum front end, the alignment of the synthetic aperture compression stage and the initial demonstration of the 1.15 PW @ 850 J operations in the compression stage are detailed. Issues encountered relating to damage to optics are also addressed.

OCIS codes: (320.0320) Ultrafast optics; (320.5520) Pulse compression; (140.3530) Lasers, neodymium.

References and links

1. E. B. Treacy, "Optical pulse compression with diffraction gratings," IEEE J. Quantum Electron. **5**(9), 454–458 (1969).
2. D. Strickland and G. Mourou, "Compression of amplified chirped optical pulses," Opt. Commun. **56**(3), 219–221 (1985).
3. C. Danson, D. Hillier, N. Hopps, and D. Neely, "Petawatt class lasers worldwide," High Power Laser Sci. Eng. **3**, e3 (2015).
4. N. Blanchot, G. Behar, T. Berthier, B. Busserole, C. Chappuis, C. Damiens-Dupont, P. Garcia, F. Granet, C. Grosset-Grange, J.-P. Goossens, L. Hilsz, F. Laborde, T. Lacombe, F. Laniesse, E. Lavastre, J. Luce, F. Macias, E. Mazataud, J. L. Miquel, J. Neauport, S. Noailles, P. Patelli, E. Perrot-Minot, C. Present, D. Raffestin, B. Remy, C. Rouyer, and D. Valla, "Overview of PETAL, the multi-Petawatt project in the LMJ facility," in *Eighth-International-Conference-on-Inertial-Fusion-Sciences-and-Applications* (IFSA, 2011), paper 07001 (2013).
5. D. Batani, M. Koenig, J.-L. Miquel, J. E. Ducret, E. d'Humieres, S. Hulin, J. Caron, J. L. Feugeas, P. Nicolai, V. Tikhonchuk, L. Serani, N. Blanchot, D. Raffestin, I. Thfoin-Lantuejoul, B. Rosse, C. Reverdin, A. Duval, F. Laniesse, A. Chance, D. Dubreuil, B. Gastineau, J. C. Guillard, F. Harrault, D. Leboeuf, J.-M. Le Ster, C. Pes, J.-C. Toussaint, X. Leboeuf, L. Lecherbourg, C. I. Szabo, J.-L. Dubois, and F. Lubrano-Lavaderci, "Development of the PETawatt Aquitaine Laser system and new perspectives in physics," Phys. Scr. T **161**, 014016 (2014).
6. J.-L. Miquel, C. Lion, and P. Vivini, "The Laser Mega-Joule: LMJ & PETAL status and Program Overview," J. Phys. Conf. Ser. **688**(1), 012067 (2016).
7. L. J. Waxer, D. N. Maywar, J. H. Kelly, T. J. Kessler, B. E. Kruschwitz, S. J. Loucks, R. L. McCrory, D. D. Meyerhofer, S. F. B. Morse, C. Stoeckl, and J. D. Zuegel, "High-energy petawatt capability for the OMEGA laser," Opt. Photonics News **16**(7), 30–36 (2005).
8. Y. Kitagawa, H. Fujita, R. Kodama, H. Yoshida, S. Matsuo, T. Jitsuno, T. Kawasaki, H. Kitamura, T. Kanabe, S. Sakabe, K. Shigemori, N. Miyanaga, and Y. Izawa, "Prepulse-free petawatt laser for a fast ignitor," IEEE J. Quantum Electron. **40**(3), 281–293 (2004).

#292261 https://doi.org/10.1364/OE.25.016957
Journal © 2017 Received 6 Apr 2017; revised 10 May 2017; accepted 11 May 2017; published 10 Jul 2017
Corrected: 25 July 2017

Optics EXPRESS

9. N. Miyanaga, J. Kawanaka, S. Tokita, T. Jitsuno, Y. Nakata, H. Shiraga, S. Fujioka, and LFEX Team, "Precision performance for full-scale operation of LFEX PW laser," in *Conference on Lasers and Electro-Optics* (2015), paper 26D1_1.
10. C. Barty, M. Key, J. Britten, R. Beach, G. Beer, C. Brown, S. Bryan, J. Caird, T. Carlson, J. Crane, J. Dawson, A. C. Erlandson, D. Fittinghoff, M. Hermann, C. Hoaglan, A. Iyer, L. Jones II, I. Jovanovic, A. Komashko, O. Landen, Z. Liao, W. Molander, S. Mitchell, E. Moses, N. Nielsen, H.-H. Nguyen, J. Nissen, S. Payne, D. Pennington, L. Risinger, M. Rushford, K. Skulina, M. Spaeth, B. Stuart, G. Tietbohl, and B. Wattellier, "An overview of LLNL high-energy short-pulse technology for advanced radiography of laser fusion experiments," Nucl. Fusion **44**(12), 266–275 (2004).
11. E. Hugonnot, G. Deschaseaux, O. Hartmann, and H. Coïc, "Design of PETAL multipetawatt high-energy laser front end based on optical parametric chirped pulse amplification," Appl. Opt. **46**(33), 8181–8187 (2007).
12. C. Dorrer and J. D. Zuegel, "Design and analysis of binary beam shapers using error diffusion," J. Opt. Soc. Am. B **24**(6), 1268–1275 (2007).
13. J. Néauport, N. Blanchot, C. Rouyer, and C. Sauteret, "Chromatism compensation of the PETAL multipetawatt high-energy laser," Appl. Opt. **46**(9), 1568–1574 (2007).
14. H. Coic, J.-P. Airiau, N. Blanchot, E. Bordenave, and C. Rouyer, "Modeling of PETAL laser chain using the Miró code," to be submitted.
15. H. T. Powel, A. C. Erlandson, and K. S. Jancaitis, "Characterization of high power flashlamps and application to Nd:glass laser pumping," Proc. SPIE **609**, 78–93 (1986).
16. D. C. Brown, *High Peak Power Nd:glass Laser* (Springer Verlag, 1981).
17. N. Blanchot, E. Bar, G. Behar, C. Bellet, D. Bigourd, F. Boubault, C. Chappuis, H. Coïc, C. Damiens-Dupont, O. Flour, O. Hartmann, L. Hilsz, E. Hugonnot, E. Lavastre, J. Luce, E. Mazataud, J. Neauport, S. Noailles, B. Remy, F. Sautarel, M. Sautet, and C. Rouyer, "Experimental demonstration of a synthetic aperture compression scheme for multi-Petawatt high-energy lasers," Opt. Express **18**(10), 10088–10097 (2010).
18. D. Bigourd, J. Luce, E. Mazataud, E. Hugonnot, and C. Rouyer, "Direct spectral phase measurement with spectral interferometry resolved in time extra dimensional," Rev. Sci. Instrum. **81**(5), 053105 (2010).
19. I. A. Walmsley and C. Dorrer, "Characterization of ultrashort electromagnetic pulses," Adv. Opt. Photonics **1**(2), 308–437 (2009).
20. G. Pariente, V. Gallet, A. Borot, O. Gobert, and F. Quere, "Space–time characterization of ultra-intense femtosecond laser beams," Nat. Photonics **10**(8), 547–553 (2016).
21. N. Blanchot, G. Behar, H. Coïc, C. Damiens Dupont, and C. Rouyer, "High precision alignment of PW compressor system for kJ-PW class laser," to be submitted.
22. C. Fiorini, C. Sauteret, C. Rouyer, N. Blanchot, S. Seznec, and A. Migus, "Temporal aberrations due to misalignments of a stretcher-compressor system and compensation," IEEE J. Quantum Electron. **30**(7), 1662–1670 (1994).
23. ISO Standard Nos. 21254–1–21254–4 (2011).
24. M. Sozet, J. Neauport, E. Lavastre, N. Roquin, L. Gallais, and L. Lamaignère, "Assessment of mono-shot measurement as a fast and accurate determination of the laser-induced damage threshold in the sub-picosecond regime," Opt. Lett. **41**(4), 804–807 (2016).
25. M. Sozet, J. Neauport, E. Lavastre, N. Roquin, L. Gallais, and L. Lamaignère, "Study of the laser damage growth on components for high power," Opt. Express (to be published).
26. M. Sozet, J. Neauport, E. Lavastre, N. Roquin, L. Gallais, and L. Lamaignère, "Laser damage growth with picosecond pulses," Opt. Lett. **41**(10), 2342–2345 (2016).
27. M. Sozet, J. Néauport, E. Lavastre, N. Roquin, L. Gallais, and L. Lamaignère, "Laser damage density measurement of optical components in the sub-picosecond regime," Opt. Lett. **40**(9), 2091–2094 (2015).

1. Introduction

The invention of optical pulse compression with diffraction gratings by Treacy [1] and the advent of the Chirped Pulse Amplification (CPA) technique in 1985 [2] paved the way to ultra-high intensity large laser facilities devoted to the study of light-matter interactions. Since the end of the nineties, several ultra-high intensity systems have been built and commissioned around the world as upgrades of older systems or new facilities to reach the PW [3]. The Petawatt Aquitaine Laser (PETAL) beamline has been designed and constructed by the French Commissariat à l'énergie atomique et aux énergies alternatives (CEA) to deliver laser pulses in the kJ-picosecond range at a wavelength of 1053 nm [4]. PETAL will allow for experiments in the field of ultrahigh intensity sciences, extreme plasma physics, astrophysics, radiography, and for fast ignition by a combination of its own multipetawatt kilojoule beam and the nanosecond multikilojoule beams of the Laser Megajoule (LMJ) [5,6]. The PETAL beamline hence joins kJ-ps range, Petawatt to multi-Petawatt facilities such as OMEGA-EP [7], LFEX [8, 9] or NIF-ARC [10]. In this paper, we present the laser commissioning of the PETAL beamline and its main current performances. In particular, we detail the front-end

Optics EXPRESS

performance (Section 2), the kJ shots performed in the amplifier section with a large spectrum front end (Section 3), and the alignment and diagnostics used for the synthetic aperture compression scheme (Section 4). Finally, we present the first 1.15 PW shot in the compression stage performed in May 2015. This 1.15 PW shot makes PETAL one of the most powerful single beams in operation in the world [6]. We also detail damage observed on vacuum optics operating in the short pulse regime (gratings, mirrors) and developments applied to improve this damage barrier. PETAL energy is limited to 1 kJ at the beginning of the laser operation due to the laser damage threshold of the final optics. Higher energy levels will be reached when working on the final optics based on the principles detailed hereinafter.

2. Front-end performance

The front-end of PETAL [Fig. 1] [11] is based on two optical parametric amplification (OPA) stages pumped by a 4.5 ns, 1.2 J custom-built laser at a wavelength of 526 nm with spatio-temporal shaping. A seed pulse is provided by a mode-locked oscillator delivering 100 fs pulses at a wavelength of 1053 nm, subsequently stretched by a single grating and an all-reflective Öffner system. To obtain the 0.5625 ns/nm stretching ratio required for seeding the amplifier section, the 16 nm FWHM spectral bandwidth pulses are stretched up to 9 ns. The pump pulse is then significantly shorter than the seed pulse. Actually, because of the large OPA gain and spectral narrowing in the amplifier section, this discrepancy can be neglected. The saturation of the parametric amplification achieves the required tailoring and delivers an amplified signal of 4.5 ns @ 8 nm, and 80 mJ [Figs. 1 and 2] before beam shaping. Finally, the beam is shaped using an apodizer to create a square beam. A phase plate using error diffusion [12] is then used before the last spatial filter of the front-end to shape the 4 sub-aperture beam into a square beam [Fig. 2], as required by the compression scheme. The energy of the front-end injected into the amplifier section is then 60 mJ.

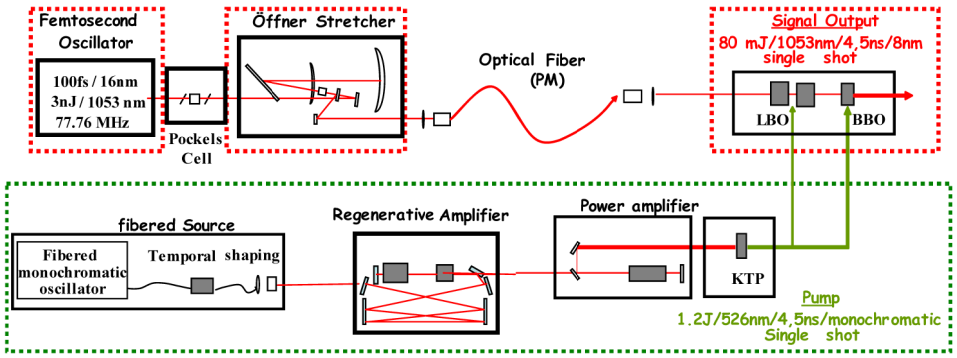

Fig. 1. Front-end schematic view.

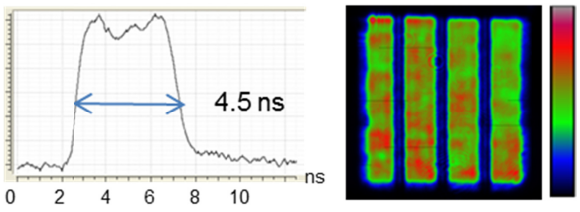

Fig. 2. Temporal profile and spatial profile at 60 mJ and 8 nm.

3. Amplifier section performance

The PETAL amplifier section is designed to deliver energy of 6.4 kJ at a wavelength of 1.053 µm. The amplifier section has the same laser architecture as the LMJ amplifier section,

Optics EXPRESS

however the 4x2 beams amplifier section mechanical structure of the LMJ is modified to handle a single beam (37.1 x 35.6 cm^2). The architecture comprises a four-pass system with angular multiplexing and a reverser [Fig. 3]. It uses 16 amplifier laser slabs arranged into two sets. The front-end pulse is injected into the transport spatial filter, passes into two amplifier groups separated by the cavity spatial filter, bounces off the M1 deformable mirror, and passes through the 16 slabs a second time. The beam is then reflected off the Mdt1 mirror, enters the reverser, reflects off the M2 mirror and goes back to M1 to exit the amplifier section after L4, the last transport spatial filter lens.

The two sets of amplifiers can accept up to 9 slabs. For 6.4 kJ operations, only 16 slabs are required. Therefore, PETAL uses 7 (cavity amplifier) and 9 (transport amplifier) Phosphate Nd:glass slabs, 8 from HOYA (LHG-8) and 8 from SCHOTT (LG-770) to optimize the spectral bandwidth taking benefit of the small fluorescence peak difference (0.4 nm).

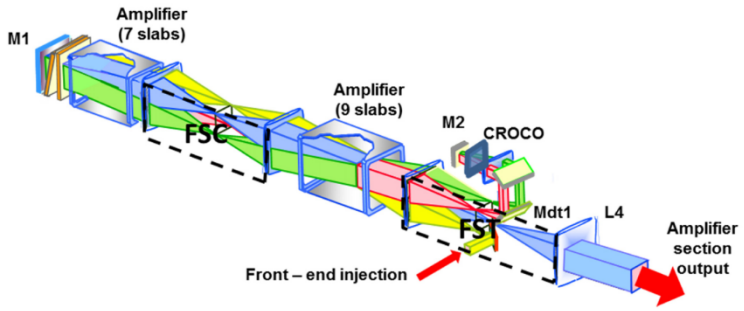

Fig. 3. Amplifier section scheme.

These spatial filters (pair of refractive lenses) are used to clean the beam of unwanted intensity modulations at high spatial frequencies and also to extend and/or to image the spatial profile for each amplifier stage. As glass index depends on wavelength, when a polychromatic light goes through a refractive lens, this light is focused in multiple foci along the lens axis, each corresponding to a given wavelength. This aberration is known as longitudinal chromatic aberration or Pulse Front Curvature. This chromatic aberration is equivalent to a delay in the time domain and the addition of the delays induced by traversing the various lenses of the Amplifier Section (equivalent to 1520 fs) will prevent the system from reaching sub-picosecond compression if uncorrected. We have consequently fitted a chromatism corrector [13] in the reverser. This chromatism corrector (CROCO) uses a diffractive Fresnel lens with a focal length of 2.523 m, in combination with a divergent refractive lens allowing for a correction of −1520 fs.

The amplifier section was commissioned in two steps. The first step was performed with an LMJ front-end delivering monochromatic pulses and a full aperture, to qualify the gain of the different slabs in the single-beam configuration. The second step was performed with the PETAL front end (large spectrum and sub-aperture beam) to study the effect of spectral gain narrowing and observe the evolution of the sub-aperture beam profiles.

Monochromatic commissioning demonstrated energy of 4.9 kJ in 5 ns, corresponding to LMJ pulse duration operation. To remain within the range of PETAL in terms of pulse duration and energy, 1.9 kJ in 1.7 ns was qualified.

Large spectrum commissioning demonstrated energy of 1.4 kJ in 2 ns with a 3.5 nm spectral bandwidth and a sub-aperture shaped beam. The decrease in pulse duration is due to spectral gain narrowing in the Nd:glass amplifiers. This output energy value corresponds to the current operating point since 1.4 kJ corresponds to 1 kJ after compression. This is the maximum energy level we can compress due to the damage threshold after the compressor. This large spectral bandwidth was commissioned with 13 slabs, to limit the energy stored in

Optics EXPRESS

the amplifiers. Adding up to 16 slabs will allow 6 kJ in extracted energy to be reached, corresponding to the initial specification.

All the shots realized during the commissioning of PETAL are plotted in the next two figures. The first figure [Fig. 4] corresponds to commissioning with monochromatic pulses, which allowed amplifier slab gain to be adjusted. Simulations use the Miró code [14] and the 2D-gain profile calculated with the Amp3D code [15].

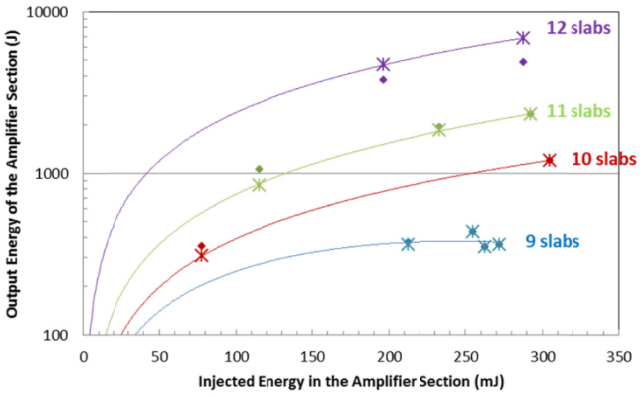

Fig. 4. Output energy of the amplifier section versus injection energy and number of slabs activated for monochromatic pulses. Dots are experimental results; crosses are Miró simulations and lines are best fits for the Miró simulations.

The next figure [Fig. 5] presents shots with large spectrum pulses (4.5 ns @ 8 nm super Gaussian front-end pulses). The maximum gain values have been fixed taking monochromatic shots into account. In these initial large spectrum simulations, spectral gain is modeled by a 14 nm Lorentzian profile centered at 1053 nm or 1053.4 nm, depending on the slab vendor (LHG-8 or LG-770). We observe a lack of energy in the Miró simulations for configurations with fewer slabs. The differences between Miró and experimental results are partially due to the spectrum of the amplifier media and could come from the spectral transmission of the amplifier section (polarizer, …). The spectral gain of phosphate is more complex than a Lorentzian [16]. Moreover, the dispersion in the experimental points is due to front-end fluctuation (spectral and spatial profiles) and each experimental point should be simulated with the precise measurement of the injected beam for better accuracy.

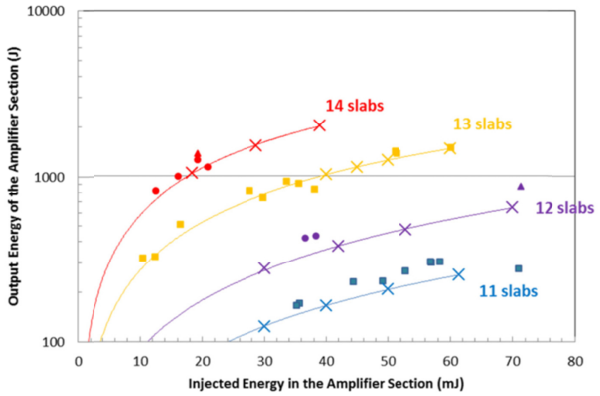

Fig. 5. Output energy of the amplifier section versus injection energy and number of slabs activated for large spectrum pulses. Dots are experimental results; crosses are Miró simulations and lines are best fits for the Miró simulations.

Optics EXPRESS

Commissioning results with a sub-aperture beam are presented in Fig. 6 with the evolution of the temporal and spatial profiles for the 1.15 PW shot. 14 slabs were used to amplify the beam from 20 mJ to 1240 J.

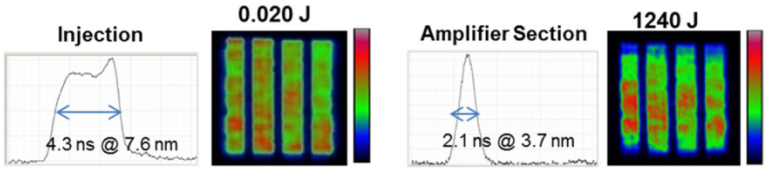

Fig. 6. Sub-apertures beam amplification up to 1.24 kJ.

These commissioning processes have indicated [Fig. 7] that the holes in the beam are affected neither by the ASE in the amplifiers nor by amplification saturation. We observe a deformation of the spatial profile along the sub-apertures due to the amplifier gain. A new phase plate has been designed to compensate for this shape and will be implemented in PETAL for future shots to obtain a top hat spatial profile and extract more energy for the same maximum fluence.

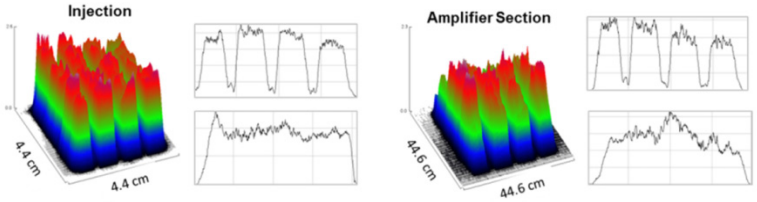

Fig. 7. Profiles of the injected and the amplified beam.

4. Compression performance

4.1 Compression scheme

The PETAL compressor scheme [17] is based on the coherent addition of beams instead of grating mosaic phasing. The initial beam is divided into sub-apertures, which are independently compressed and synchronized with classical (micrometric range) precision. Finally, these sub-apertures are coherently combined using only one segmented mirror with three interferometric displacements for each sub-aperture. To limit the volume of the vacuum compressor, compression is applied in two stages [Figs. 8 and 9]. First, a compressor in air reduces pulse duration from a few nanoseconds to a few hundred picoseconds in an unfolded double pass compression configuration (gratings G11, G12, G13 and G14). The relatively long pulse duration allows for the use of 83 cm monolithic gratings by decreasing the grating incidence angle. Second, a compressor in a vacuum finalizes the compression of the pulse down to a duration of 500 fs. The second compression stage is designed with a small compression factor to limit transverse chromatism in a single-pass configuration. This allows us to consider this compressor as four independent units, each one addressing one sub-aperture. Each independent compressor (G21/G22, G23/G24, G25/G26 and G27/G28) may even have different characteristics such as groove density or incidence angle. Finally, a segmented mirror between the two compression stages compensates the spatial phase shift induced by the separation of the gratings in the final compressor. The first compressor has a groove density of 1680 g/mm, an incidence of 56° and a grating distance of 2.62 m. The second compressor has a groove density of 1780 g/mm, an incidence of 77.2° and a grating distance of 2 m. The transmission is 81% for the first stage of compression and 91% for the second stage.

Optics EXPRESS

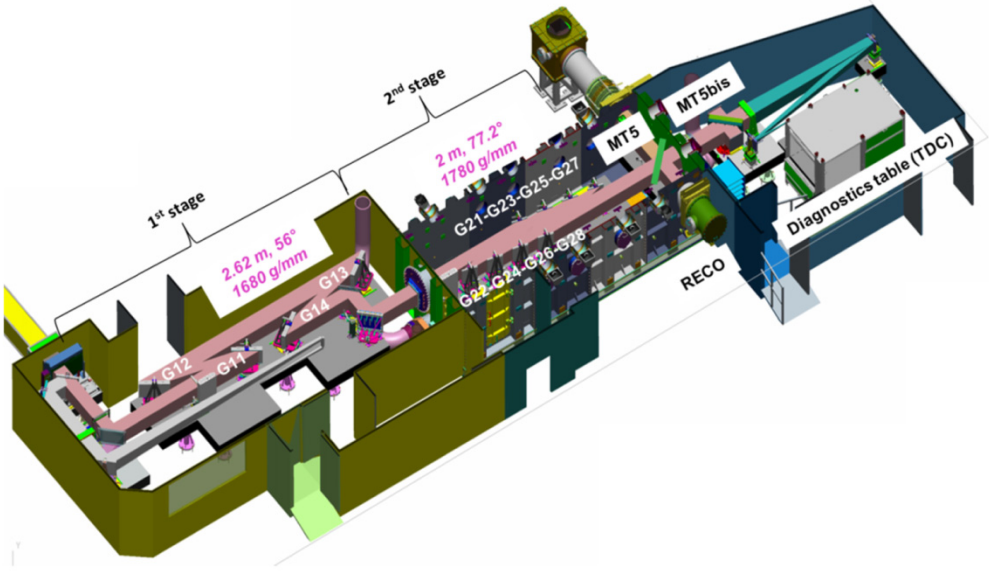

Fig. 8. Implementation of the compression stage and diagnostics table (TDC); MT5 and MT5bis are drawn in target shot configuration.

Fig. 9. 1st stage of compression in air (left), 2nd stage of compression in the vacuum vessel (center) and compression diagnostics table (right).

4.2 Compression diagnostics

All compression diagnostics are performed after a pair of leaky mirrors, MT5 (transport mirror #5) and MT5bis [Figs. 8 and 9]. These 2 mirrors have 3 configurations: shot on target (+ 45°, –45°), shot on the compression calorimeter (–45°, + 45°), and alignment (+ 1°, –1°). These configurations allow for transmission to be adjusted while maintaining the same beam centering. MT5 has 0.16% transmission at an incidence of 45° and more than 60% at 0°. MT5bis has 3% transmission at 45° and more than 60% at 0°.

Spatio-temporal effects are some of the key issues for the ultra-high intensity beam [19, 20]. Therefore, many efforts were made in terms of image relay and beam propagation prior to the diagnostics. A diffractive lens is used to compensate for longitudinal chromatism in the diagnostic pickup and the beam is imaged in the different diagnostics. Multiple characteristics of this attenuated beam are measured on the compression diagnostics table (TDC): the near field, the far field, the pulse duration with a second order autocorrelator, the spectrum, the spectral phase with a SPIRITED [18], spectral phase differences and the synchronizations between sub-aperture pulses with a 2D spectral interferometer (2D-SI) [17] and the relative energy. An absolute calorimeter for energy (RECO) is installed in a specific vacuum box to calibrate the relative energy. All diagnostics can be performed in single-shot operation.

The 2D-SI [17] uses a bi-prismatic plate, a cylindrical lens for one-direction focusing along the slit axis (vertical axis), and a spectrograph with a 0.05 nm spectral resolution. The temporal delay between the sub-apertures is visually deduced and precisely adjusted by

Optics EXPRESS

analysing the interference pattern using a 1D-Fourier transform along the slit axis. Moreover, a visual 2D-SI pattern observation allows the differential spectral phase shift to be quantified and qualified: delay, chirp difference between sub-apertures, temporal distortion and also residual unwanted dispersion.

Figure 10 shows the 2D-SI for the full beam, with 4 sub-apertures corresponding to the 4 independent compressors of the second stage of compression. In the first image, sub-apertures are not synchronized, therefore we observe a complex system of vertical fringes. After adjusting the grating distances of the 3 sub-apertures to be synchronized, we observe only one system of vertical fringes, which corresponds to one independent compressor not synchronized with the 3 others. By finally adjusting the distance of this 4th independent compressor, we suppressed the last vertical fringes. A small curvature (SMILEY) was observed in the horizontal fringes due to residual chirp difference, horizontal fringes are due to the bi-prismatic plate.

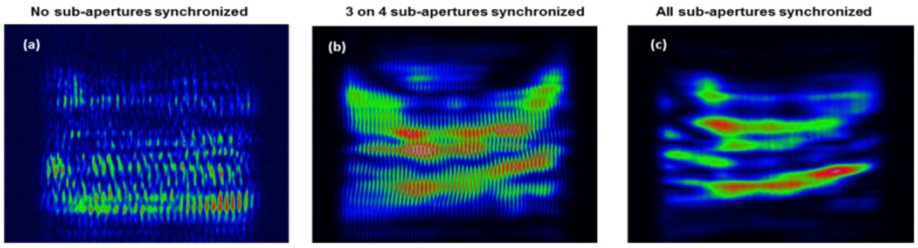

Fig. 10. 2D-spectral interferometry with 4 non-synchronized sub-apertures (a), 3 out of 4 sub-apertures synchronized (b), all sub-apertures synchronized (c).

4.3 Compressor alignments

First, each grating in the compressors (1st and 2nd stages) is pre-aligned with a monochromatic alignment laser to adjust the parallelism of the face and the grooves. The oscillator (16 nm and 77.76 MHz) from the front end is then used to precisely correct all residual angular dispersions (groove parallelism, grating face parallelism, groove density mismatch and longitudinal chromatism) [21, 22].

The sub-aperture PETAL compression scheme requires a specific alignment procedure. Indeed, the second stage is equivalent to 4 independent compressors that must be compressed and synchronized. The sub-aperture synchronization cannot be adjusted with the segmented mirror, its correction range in delay is too limited.

Since the compression is optimized (pulse duration) with a few 100 µm of grating distance adjustments and synchronization (precision 50 fs) is achieved with a few 10 µm, the PETAL compressor can be optimized in 3 steps:

- Step A: optimization of the 4 independent compressors with the second order autocorrelator. At this step, the sub-apertures have time delays T_D between each other. Vertical fringes are observed on the 2D-SI [17] due to the delay between sub-apertures [Fig. 11(a)];
- Step B: one sub-aperture is taken as a reference and a second compressor is synchronized ($T_D = 0$) with this reference by adjusting the grating distance δL^B using the 2D-SI measurement for these 2 sub-apertures. At this step, the second compressor is no longer compressed due to the grating distance displacement. A SMILEY is observed on the 2D-SI due to residual chirp [Fig. 11(b)];
- Step C: starting from step A, the gratings of the second compressor are tilted to an angle Δi^C and the grating distance changed by δL^C to compensate for both the delay and

Optics EXPRESS

the chirp. Only horizontal fringes are observed on the 2D-SI due to the bi-prismatic plate [Fig. 11(c)].

Using the second stage compressor characteristics (N = 1780 g/mm, i = 77.2°), the adjustment of each independent compressor is given by the following equations [21, 22]:

$$\delta L^C\left(\mu m\right) = 2.71 \cdot \delta L^B\left(\mu m\right) \quad (1)$$

$$\Delta i^C\left(\mu rad\right) = 0.26 \cdot \delta L^B\left(\mu m\right) \quad (2)$$

Figure 11 shows the 2D-SI results observed in the 3 alignment steps with compensation of residual chirp difference while maintaining synchronization.

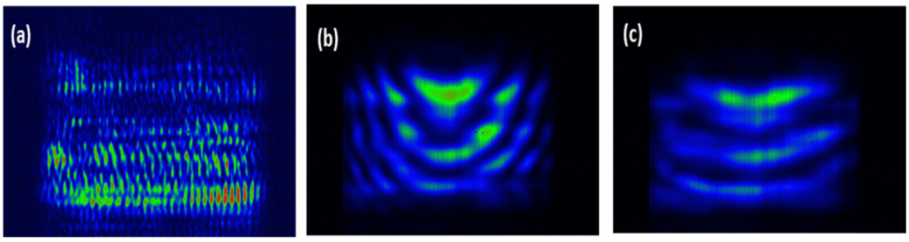

Fig. 11. Step A: 2D-spectral interferometry with 4 non-synchronized sub-apertures (a), Step B: observation of a SMILEY after synchronization of G23/G24 pulse with G25/G26 (b), Step C: reduction of the SMILEY with changes of incidence angle and grating distance of G25/G26 (c).

A small global residual chirp may persist after these 3 steps. This global chirp is then suppressed using a monolithic grating in the 1st stage of compression to correct the 4 sub-apertures at the same time. This fine adjustment is measured using the SPIRITED [18].

4.4 Experimental results to demonstrate a peak power of 1.15 PW

4.4.1 Compression

Compression can be optimized by changing the grating distances of each independent compressor. Pulse duration is measured with a second order autocorrelator. Figure 12 shows the autocorrelation between the 4 independent compressors on a 219 J shot with a pulse duration between 540 fs and 570 fs for a 3 nm spectral bandwidth.

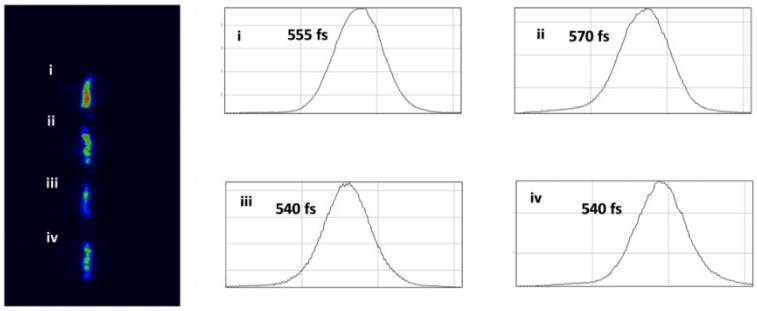

Fig. 12. Autocorrelation plots for a 219 J @ 3nm shot and pulse durations at FWHM.

4.4.2 Synchronization of sub-aperture pulses with compression maintained

Figure 13 presents the experimental results obtained for 2 independent compressors (G25/G26, G27/G28) by taking compressor G23/G24 as a reference. First, the 2D-SI measurements [Fig. 13(a)] give SMILEY at best synchronization, which is an indication of residual chirp difference. The formula given by Eq. (1) and Eq. (2) are used to correct this

Optics EXPRESS

chirp difference and to maintain synchronization [Fig. 13(b)]. The improvements for autocorrelation plots are shown in Figs. 13(c) and 13(d).

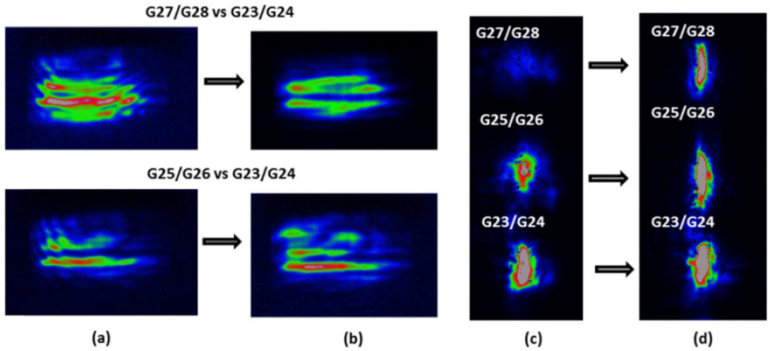

Fig. 13. (a) 2D-SI with the residual chirp; (b) 2D-SI after modifications of gratings angle and grating distance; (c) and (d) 2nd order autocorrelation traces corresponding to (a) and (b).

The 2D-SI is more precise (interferometric precision $\Delta\varphi_{2nd\ order}(\omega) << 2\pi$) to optimize the relative chirp between independent compressors than the second order autocorrelator. Moreover 2D-SI has the advantage to allow measurement with the oscillator pulse train instead of the mJ front-end pulse (1 shot / 4 min). Synchronization better than +/– 50 fs between sub-apertures could be obtain thanks to this 2D-spectral interferometer.

4.4.3 1.15 PW shot

During the first PW campaign in may 2015, the measurements on the TDC was biased by Kerr effect due to the propagation in the diagnostic pick-up and by an imperfect relay imaging on the diagnostics. All these points are now improved [Fig. 12]: imaging systems are under vacuum, near fields are imaged on diagnostics, energy on the TDC is limited to 3 mJ (15 mJ on the 1.15 PW shot). Moreover, we have decided to completely model the diagnostics using Miró code to take into account the residual Kerr effect and the spatio-temporal effects on measurements. This point is crucial since the maximum peak power is less than the direct ratio of the energy divided by the pulse duration deduced from the autocorrelation measurement.

Before the maximum energy shot, we delivered a front-end shot [Figs. 14 and 15] to validate the compression performance (400 fs for the 8 nm supergaussian profile). The input for Miró simulations come from experimental measurements of the beam at the amplifier section injection (spatial, temporal, spectral profiles). We find a quite good agreement between the experimental results and the simulations. The Miró code allows us to add the residual synchronization of the sub-apertures [Fig. 15(d)] to estimate the pulse duration with more accuracy.

Optics EXPRESS

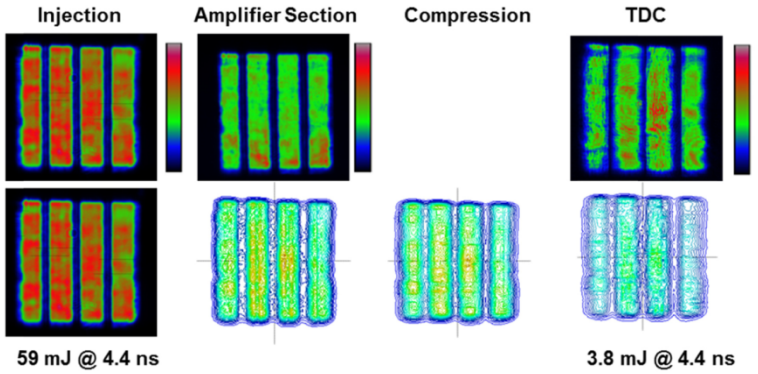

Fig. 14. Spatial experimental (top) and simulated (bottom) profiles for the front-end shot.

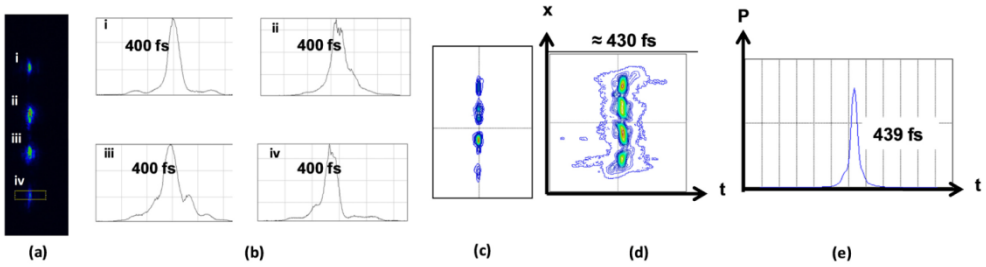

Fig. 15. Experimental (a, b) and simulated (c) 2nd order autocorrelation plots at TDC, simulated energy front profile at the output of the compressor (d) and peak power (e) for the front-end shot

The 1.15 PW shot was then run with the activation of 14 slabs in the amplifier section. These 14 slabs amplify energy from 20.3 mJ @ 4.3 ns up to 1.24 kJ @ 3.7 nm. The experimental and associated simulated profiles are shown in Figs. 16 and 17. We observe a Kerr effect on the measurements and on the simulations due to the level of energy injected at TDC, 15 mJ instead of 3 mJ (value for optimal diagnostics). The duration of the compressed pulse, with synchronization, is equal to 700 fs for an energy level of 850 J, corresponding to 1.15 PW. Energy is measured using the RECO calorimeter.

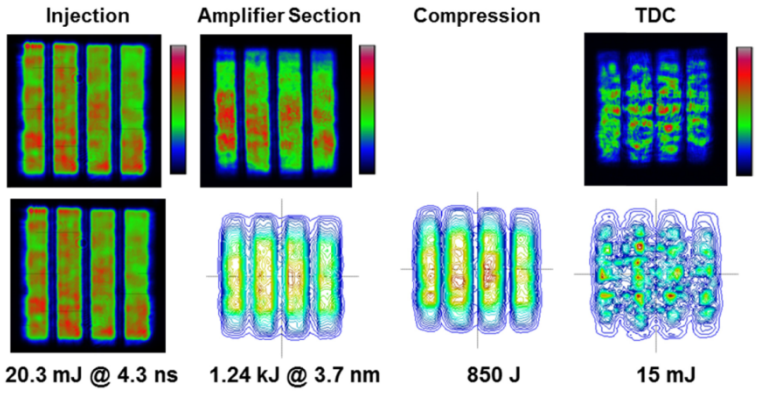

Fig. 16. Spatial experimental (top) and simulated (bottom) profiles for the 1.15 PW shot.

Optics EXPRESS

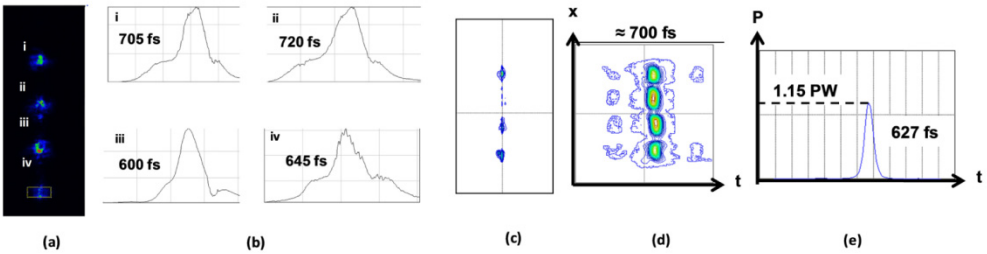

Fig. 17. Experimental (a, b) and simulated (c) 2nd order autocorrelation plots at TDC, simulated energy front profile at the output of the compressor (d) and peak power (e) for the 1.15 PW shot.

Moreover this shot was also measured with a damaged leaky mirror [Fig. 18(a)] inducing a reflection decrease of 8.8% for the calorimeter. Hence, the real energy on this shot was 925 J instead of 850 J, which corresponds to 1.25 PW.

4.5 Damage issues

Visual inspections were carried out during the PETAL beamline commissioning process to check for potential laser damage. Pulse compression gratings and the MT5 leaky mirror after were pictured after compression using observation windows located in the vicinity of these optical components. We particularly focused on leaky and transport mirrors. Pulse compression gratings are used at a 77.2° incidence while mirrors operate at 45°. The latter are therefore likely to be the first to exhibit laser damage, the beam size on the component surface is 3 times higher for the gratings due to the incidence angle.

Initial damage was detected on the MT5 leaky mirror above a power of approximately 0.8 PW ($F_{max} \approx 1.3$ J/cm^2, in beam normal) during the first PW campaign where the MT5 was oriented using the RECO calorimeter and no damage was observed for gratings. Damage occurred at a relatively low energy level due to both the excessive beam spatial modulations and a non-optimized early coating design. We then first worked on the mirror coating design.

We also decided to test the transport mirror MT6 (transport mirror next to MT5). To this end, the MT6 component was placed in the MT5 position. Figure 18 shows the damage pattern observed for these optical components. Rather large areas of each sub-aperture exhibit damage morphology typical of intrinsic material damage, suggesting that the mirror damage threshold was locally exceeded. Moreover, the high spatial frequency patterns observed in Fig. 18 are likely to be induced by the diffraction gratings and their manufacturing process.

Based on these results, we modified the coating design to enhance the laser induced damage threshold (LIDT) of the mirror while maintaining the same reflectivity. This basically involves reducing the electric field in the first layers of the coating by changing the stack design. The LIDT of samples representative of both the early and the updated design were damage tested using both a 1:1 damage procedure [23] and a mono-shot protocol using the DERIC damage tester [24]. Two improvements were revealed, for example, for the MT5 leak mirror, raising the LIDT from 1.7 J/cm^2 to 3.7 J/cm^2 at 1.053 µm, 770 fs, 45°, S-pol in the beam normal. The MT5 leaky mirror was consequently replaced with a mirror coated with this updated design and used in the next commissioning steps.

Optics EXPRESS

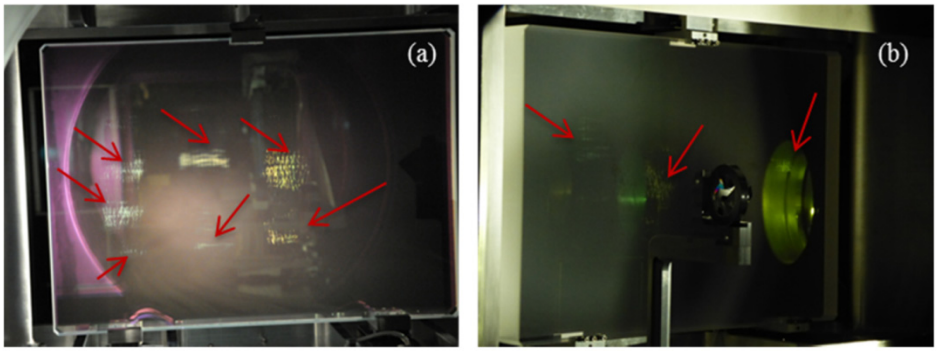

Fig. 18. MT5 leaky mirror, early design, after a 572 J, 700 fs shot May 2015 (a) MT6 transport mirror, early design, after a 1004 J, 1 ps shot, October 2015 (b). Damage to sub-apertures (red arrows)

A visual inspection after a 1 PW shot on the MT5 leaky mirror confirmed the trend observed for samples. As seen on Fig. 19, the mirror is now sustaining this high intensity.

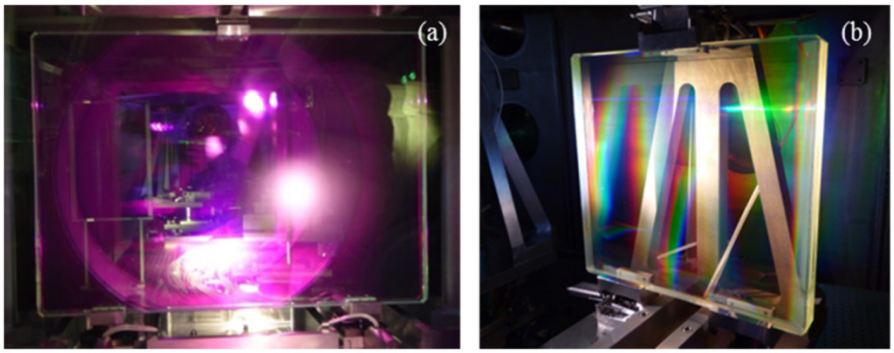

Fig. 19. MT5 leaky mirror with updated design (a) and pulse compression grating after a 1 PW shot (1030 J, 1 ps) (b). October 2015. No damage observed visually.

A complete optical inspection was performed in the metrology lab on the MT6 early design mirror after replacement. This inspection confirmed that most damage was intrinsic, with damage sites growing during successive laser shots [25]. Nevertheless, sparse localized coating defects, induced damage, were also observed. Their morphology is similar to that already seen on mirror samples and these are also growing sites, as reported elsewhere [26]. While the intrinsic damage threshold can be measured with a 1:1 damage testing protocol, coating defect induced damage (which remained well below the 1:1 threshold) is measured using a raster scan testing protocol [27]. Both intrinsic threshold and damage density must be improved to reach the multi-PW regime.

Finally, we report that during the beamline commissioning process, we observed very few localized damage sites on the pulse compression gratings. The high incidence of the gratings used in the PETAL compressor is very favorable in terms of damage resistance compared to mirrors.

Damage to optics can be induced by inadequate design or a local initiator. Beam spatial quality also has to be improved to reach a higher intensity. Knowledge of the uniformity of the beam profile, beam modulations and beam size must be improved.

All of these contributions are options in order to reach the 2 PW target.

Optics EXPRESS

5. Summary

The PETAL beamline was commissioned over a 2-year period up to the end of the compressor stage. During this commissioning process, the amplifier section demonstrated its ability to deliver energy up to 5 kJ and a spectral bandwidth up to 3 nm, compatible with 500 fs operation. Spatial beam shaping was managed with a phase plate in the front-end to create the 4 sub-apertures required for the compression stage. This beam shaping process is not affected by the ASE during the high energy amplification process. A PW campaign was then carried out on the PETAL beamline in May 2015. A 1.15 PW shot was obtained with 700 fs pulse duration and 850 J energy at the output of the PETAL compressor. Attention was paid to the compressor alignment, on beam pickup and during diagnostics to limit non-linear and spatio-temporal effects. Full-scale optics (transport mirrors in particular), visual monitoring and sample damage testing indicated that the first transport mirror design was limited to 1.7 J/cm^2. The new coating design with a damage threshold of 3.7 J/cm^2 has been validated in transport allowing for the future transport of 1 kJ in the target chamber. Furthermore, works are in progress to optimize the spatial beam profile to obtain a more uniform beam.

Funding

This work is being performed by the Commissariat à l'énergie atomique et aux énergies alternatives under the financial auspices of the Aquitaine Region in France (project owner), the French Government and the European Union.